

# RADIOACTIVE BEAM ACCUMULATION FOR A STORAGE RING EXPERIMENT WITH AN INTERNAL TARGET

F. Nolden, C. Dimopoulou, R. Grisenti, C. Kleffner, S. Litvinov, W. Maier, C. Peschke, P. Petri, U. Popp, M. Steck, H. Weick, D. Winters, T. Ziegler, GSI, Darmstadt, Germany

## Abstract

A radioactive  $^{56}\text{Ni}$  beam was successfully accumulated for an experiment with an internal hydrogen target at the storage ring ESR of GSI, Germany. The radioactive beam was produced and separated at the GSI fragment separator from a stable  $^{58}\text{Ni}$  beam. About  $8 \cdot 10^4$   $^{56}\text{Ni}^{28+}$  ions were injected into the ESR on a high relative momentum orbit. The beam was subjected to stochastic precooling, bunched and transported to a low relative momentum orbit. Slightly below this deposition momentum, the beam was accumulated and continuously cooled by means of electron cooling. After accumulating about 60 shots, this beam was prepared to overlap with the ESR internal gas jet target for a nuclear physics experiment. Data acquisition was started with a stored beam of roughly  $4.8 \cdot 10^6$  particles in the beginning.

## OVERVIEW

A radioactive  $^{56}\text{Ni}^{28+}$  beam was accumulated for the first time in the ESR to an amount which was sufficient for performing a nuclear physics experiment with the ESR internal target. A proof of principle experiment had already been performed in 1999 [1]. The final success of the experiment was due to the large acceptance of the ESR, the application of both stochastic and electron cooling, and the versatile orbit bumps, which are available at the ESR, both in the horizontal and in the vertical directions.

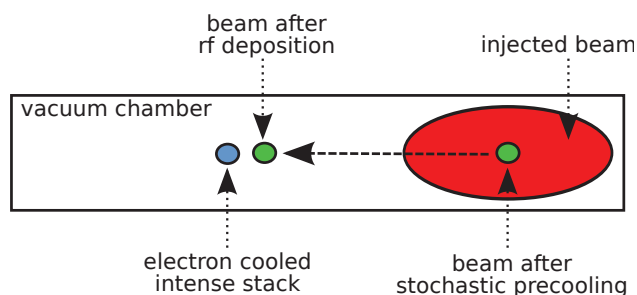


Figure 1: Scheme of beam orbits during accumulation.

The beam was prepared for the experiment by sequentially performing the following procedures:

1. Acceleration of a primary  $^{58}\text{Ni}^{28+}$  beam in the SIS18 synchrotron with fast extraction.
2. Production of the secondary  $^{56}\text{Ni}^{28+}$  ions at a fragmentation target in the fragment separator FRS [2].

3. Fast kicker injection into the Experimental Storage Ring ESR.
4. Stochastic precooling and bunching with dedicated orbit bumps.
5. Displacement by rf to an inner orbit with a special vertical orbit bump.
6. Displacement of the deposited beam by electron cooling to a stack orbit nearby.
7. Repetition of steps 1 to 6 until a sufficient number of  $^{56}\text{Ni}^{28+}$  ions was accumulated.
8. Interaction with the internal target using dedicated target bumps. Beginning of data acquisition.

Some of these steps are sketched in Fig. 1. The beam was accumulated using up to 60 single injections. The average time between injections was 36 s, as the SIS synchrotron had to serve several different experiments in parallel.

## SECONDARY BEAM PRODUCTION

$^{56}\text{Ni}$  is a doubly-magic nucleus and its production cross section is particularly large. It is therefore best suited for a first experimental test of the general procedure. The  $^{56}\text{Ni}^{28+}$  ions were produced in the fragment separator (FRS) by shooting an intense 600 MeV/u  $^{58}\text{Ni}^{28+}$  beam from the SIS18 synchrotron on a fragmentation target. Typically  $8 \cdot 10^4$  ions were injected at each shot from the SIS. The production efficiency is roughly  $1 \cdot 10^{-4}$  per primary ion. From the secondary ions produced only 10% can be stored in the ESR, because its injection acceptance is limited. By proper settings of the FRS degrader, contaminants like  $^{54}\text{Co}^{27+}$  could be reduced to a total fraction of  $< 10^{-3}$ , reliably measured by the well-established technique of Schottky mass spectrometry [3].

## STOCHASTIC PRECOOLING

The beam in the ESR was precooled in two steps by stochastic cooling using the newly established time-of-flight method [4] in longitudinal phase space. After comparative studies of the three longitudinal stochastic cooling techniques the time-of-flight method was chosen because it is faster than the Palmer technique and has a larger momentum acceptance than notch filter cooling. In the future it is planned to provide fast switching from time-of-flight to notch filter cooling, but this was not yet available at the

time of the experiment. The injected coasting beam was cooled after injection for 5 s, then the rf was turned on to proceed with bunched beam cooling, in order to get well-cooled bunches for the subsequent displacement by rf. Simultaneously the beam was cooled horizontally and vertically.

Figure 2 shows the second moment of the longitudinal distribution ( $\sigma(\delta p/p)$ ) during stochastic precooling of a fresh secondary beam as determined from Schottky spectra. As long as the beam is coasting  $\sigma(\delta p/p)$  is decreased by a factor of 3. Then the rf is turned on non-adiabatically. Therefore  $\sigma(\delta p/p)$  first increases slightly and is then reduced anew.

Because all stochastic precooling systems (pick-ups and kickers) are installed at high dispersion ( $D \geq 4\text{m}$ ) in the outer part of the ESR acceptance, the pick-ups get only a very small signal from the stacked beam. Therefore the performance of the stochastic cooling system is practically independent of the intensity of the accumulated stack, as long as the number of injections is less than 100. Vice versa the stacked beam is not disturbed by the stochastic cooling kicks either, because both the pick-up and the kicker systems are installed at positions with identical ion optical parameters.

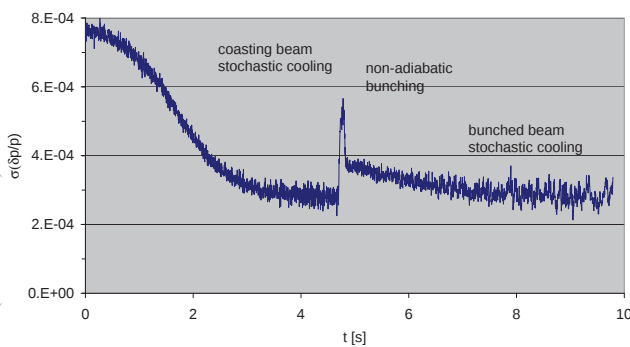


Figure 2: Momentum cooling of freshly injected beam.

## RF BEAM TRANSPORT

The precooled bunched beam was displaced by rf stacking towards an inner orbit of the ESR, where it was neither disturbed by the magnetic field of the pulsed, partial aperture injection kicker nor by the rf fields of the stochastic cooling kickers. On this orbit the beam was permanently subjected to electron cooling.

Unfortunately it was not possible to displace the beam to the inner part of the ring in a straightforward way, because a mechanical obstacle, located near the position of the kicker electrodes for horizontal stochastic cooling, was partly obscuring the acceptance [5]. However, the obstacle was only effective in the lower part of the vertical acceptance, and could be circumvented by a dedicated vertical orbit bump. Meanwhile the obstacle has been identified and removed.

Figure 3 is a waterfall diagram of Schottky spectra (124<sup>th</sup> harmonic of the revolution frequency) taken just be-

fore and after the end of the rf stacking procedure. The distance between the stack and the deposited beam ( $\delta p/p = 4.3 \cdot 10^{-4}$ ) is chosen such that the two beams are close enough for sufficiently fast merging by electron cooling. However, the stack should not be disturbed by the rf, in particular phase displacement acceleration of parts of the stack must be avoided. Therefore a low final rf voltage is advantageous, corresponding to a rather shallow bucket. An rf voltage of 200 V with a full height  $(\delta p/p)_{max} = 3.9 \cdot 10^{-4}$  was chosen. Such low voltages could be afforded because of the low momentum width after bunched stochastic precooling.

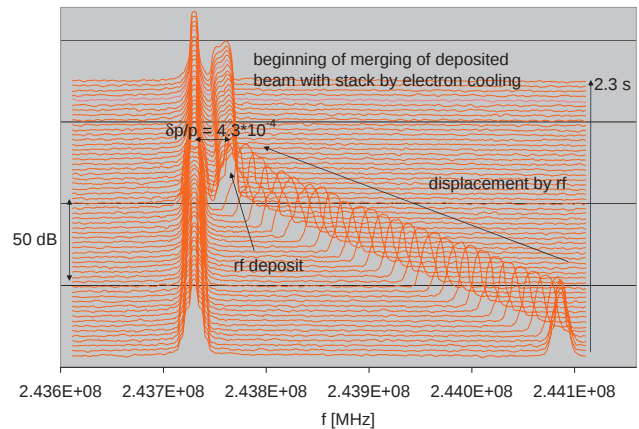


Figure 3: Schottky spectra showing the end of beam deposition and the beginning of merging the accumulated beam with the stack.

## ELECTRON COOLING

The deposited and debunched beam was gradually moved by electron cooling towards an orbit at a somewhat lower energy. It was finally merged with the stack after about 6 seconds. From the waterfall diagram shown in Fig. 4 it can be seen that the deposited beam is practically completely absorbed in the stack. After beam merging  $\sigma(\delta p/p)$  was about  $3 \cdot 10^{-5}$ , due to an equilibrium between electron cooling and intra beam scattering.

## ACCUMULATION PERFORMANCE

The total time needed for stochastic precooling and merging with the stack amounted to roughly 17 s, much less than the minimum available interval between injections at the time the experiment was performed. Neither the stochastic precooling time nor the electron cooling time were therefore critical, but may still be reduced in future experiments. Figure 5 displays a series of measured data points from the DC beam current transformer. Although its resolution is limited, the data points are rather linear, indicating that the stacking procedure was working practically lossless. The measured Schottky power intensities confirm this picture.

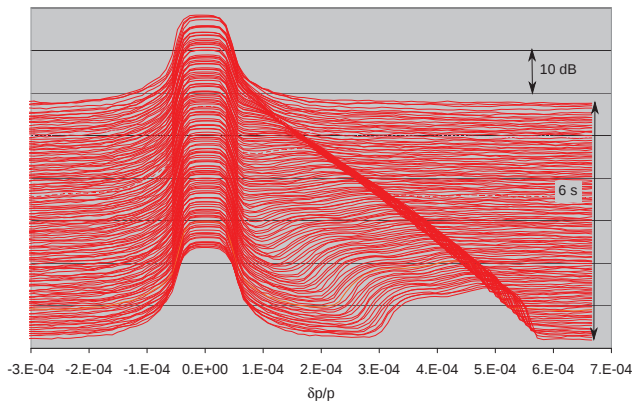


Figure 4: Schottky spectra of beam merging by electron cooling immediately after turning off the rf.

### INTERACTION WITH AN INTERNAL TARGET

Typically  $4.8 \cdot 10^6$  secondary  $^{56}\text{Ni}^{28+}$  ions interacted with the internal target after properly aligning the ion beam with the (hydrogen or helium) gas jet. The overlap between the target and the ion beam was measured in two ways. Firstly, by two scrapers located at 3 m distance before and after the interaction point, such that both the position and the direction of the beam can be controlled. Secondly, the interaction of the beam with the target leads to an average energy loss, which is usually compensated by electron cooling. However, this energy loss can be determined easily by Schottky spectroscopy. First electron cooling is switched off, and then the revolution frequency shift after a given time interval is measured. The energy loss as a function of the orbit bump at the target position is then maximized, yielding a sensitive beam-based optimization procedure, independent of any assumptions about the target geometry.

Figure 6 shows the measured relative momentum shift  $\delta p/p$  as a function of the deviation  $\delta x$  from the central orbit bump  $\delta x = 0$ , which had been determined by the scraper measurements. The data arise by folding the beam width with the target width. The corresponding beam width had been measured by scraping to be smaller than 1 mm. Hence

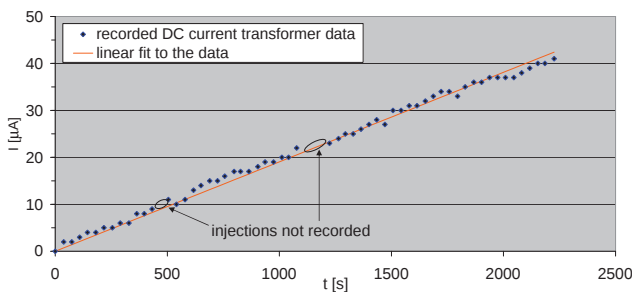


Figure 5: DC beam current transformer data plotted as a function of time. The straight line is a linear fit to the data.

the curve in Fig. 6 represents mainly the horizontal target density distribution. The data can be nicely described by a Gaussian

$$\delta p/p = d_0 \exp\left(-\frac{(\delta x - x_0)^2}{2\sigma_x^2}\right)$$

with  $\sigma_x = 2.7$  mm. The Gaussian fit value  $x_0 = 0.6$  mm indicates that the target position was close to the position determined by scraping.

Throughout the experiment the internal target [7] worked very reliably at a density of roughly  $6 \cdot 10^{12} \text{ cm}^{-2}$  (hydrogen molecules or helium atoms). With the target running, the beam halflife was about 20 min, such that the available beam time was shared almost equally between accumulation and target interaction.

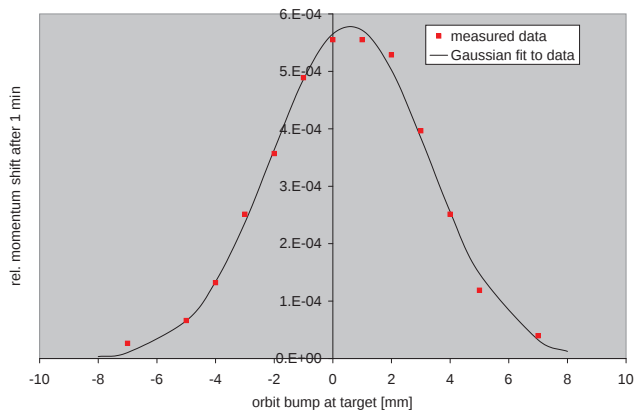


Figure 6: Beam momentum loss due to interaction with the internal target as a function of the local horizontal orbit bump.

### ACKNOWLEDGEMENT

We gratefully acknowledge the collaboration with P. Egelhof, S. Ilieva, N. Kalantar, and O. Kiselev, and thank them for providing the data of Fig 6.

### REFERENCES

- [1] F. Nolden et al., Proc. EPAC 2000, 1262-1264.
- [2] H. Geissel et al, Nucl. Inst. Meth. B 70 (1992) 286.
- [3] B. Franzke et al., Mass Spec. Rev. 27 (2008) 428-469.
- [4] C. Dimopoulou et al., GSI Scientific Report 2012, in press
- [5] C. Dimopoulou et al., GSI Scientific Report 2011, 470.
- [6] F. Nolden et al., Proc. EPAC 1998, 1052-1054.
- [7] N. Petridis et al., Nucl. Instr. Meth. A 656 (2011) 1.
- [8] H. Geissel et al., Nucl. Inst. and Meth. B 204 (2003) 71.
- [9] F. Nolden et al., Proc. EPAC 2006, 208-210.
- [10] M. Steck et al., Proc. IPAC 2012, 3722-3724.